Tracking the big ones : novel dynamics of organelles and macromolecular complexes during cell division and aging

Deventer, S.J. van

Chapter Three

Chapter 3:

Spatiotemporal analysis of organelle and macromolecular complex inheritance

Victoria Menendez-Benito[1], **Sjoerd J. van Deventer**[1], Victor Jimenez-Garcia[1], Marina Roy-Luzarraga[1], Fred van Leeuwen[2], Jacques Neefjes[1]

3

Proceedings of the National Acadamy of Sciences USA, Jan 2013, 110 (1): 175-180

[1] Division of Cell Biology 2 and
[2] Division of Gene Regulation,
Netherlands Cancer Institute, Amsterdam, The Netherlands

Abstract

Following mitosis, daughter cells must inherit a functional set of essential proteins and organelles. We applied a genetic tool to simultaneously monitor the kinetics and distribution of old and new proteins marking all intracellular compartments in budding yeasts. Most organelles followed a general pattern whereby preexisting proteins are symmetrically partitioned followed by template-based incorporation of new proteins. Peroxisomes belong to this group, supporting a model of biogenesis by growth and division from preexisting peroxisomes. We detected two exceptions: the nuclear pore complex (NPC) and the spindle pole body (SPB). Old NPCs are stably inherited during successive generations but remained separated from new NPCs, which are incorporated *de novo* in mother and daughter cells. Only the SPB displayed asymmetrical distribution, with old components primarily inherited by daughter cells and new proteins equally incorporated in both cells. Our analysis resolves conflicting models (peroxisomes, NPC) and reveals unique patterns (NPC, SPB) of organelle inheritance.

Introduction

Compartmentalization of specialized proteins into membrane-bound organelles and macromolecular machines constitutes an essential strategy to control biological processes such as DNA replication and protein degradation. When cells divide, the information and components required to build these intracellular compartments must be transmitted to progeny. One approach to achieving this is to share the preexisting maternal compartments between mother and daughter cells in a process known as "inheritance." The molecular mechanisms controlling inheritance of intracellular compartments have been extensively studied in the budding yeast *Saccharomyces cerevisiae* (1), as mothers can be distinguished from daughter cells. Budding yeasts divide asymmetrically, producing two cells (mother and bud) that are different in size, metabolism, and age. During mitosis in yeast, most organelles are transported from mother to bud along actin cables. This transport is mediated by class-V myosin proteins that recognize a specific receptor for each intracellular compartment, including the vacuole, mitochondria, peroxisomes, Golgi apparatus, and cortical endoplasmic reticulum (ER) (2). Two important exceptions are the nucleus and the perinuclear ER, which are transported by microtubules (3). Following transfer into the bud, some organelles such as cortical ER (4), mitochondria (5), and peroxisomes (6) become anchored at the bud tip, and this retention regulates the total amount of maternal components that enters the bud.

In addition to sharing preexisting compartments derived from the mother, new proteins are synthesized to support cellular growth. In principle, new components may either be incorporated into preexisting compartments or generate new copies without a template (*de novo*). Some membrane-bound compartments may only be generated in a template-based manner. For instance, many of the constituent proteins of the ER require a mature and functional translocon and chaperone system for their own synthesis. This may also be expected for other organelles such as mitochondria, which incorporate proteins made by cytosolic ribosomes. Other organelles may use the ER as a platform to generate essential components in a *de novo* fashion. Recent studies describing *de novo* formation of peroxisomes (7–10) and Golgi (11) have reopened the debate regarding organelle

biosynthesis by division and partitioning.

Another unresolved issue pertaining to protein inheritance is whether mother and daughter cells have an equal proportion of new and old components. Several examples of asymmetrical segregation have been documented. Specifically, damaged proteins accumulate in mother cells by an active retention mechanism for protein aggregates (12). Plasma membrane transporters are also distributed asymmetrically, with the old pool predominantly remaining in the mother cell (13). Recently, a nuclear transport factor was discovered that preferentially segregates to the bud, thereby redirecting translation into the daughter cell (14). It is unclear whether these examples specify specialized cases or general mechanisms for discrimination and differential segregation of old and new proteins. In such a model, newly made proteins, which may be less damaged but also less validated in functional terms, would concentrate in daughter cells. A different premise would be that old and new proteins are shared during cell division, resulting in two new cells with proteomes reset to the same molecular age.

Here we address these questions using a unique fluorescence-based system called "recombination-induced tag exchange" (RITE) (15, 16). RITE is specifically designed to distinguish and simultaneously monitor endogenous expression of old and newly synthesized proteins. Combining RITE with yeast genetics allows a global analysis of the inheritance of protein components of all intracellular compartments. Old and new proteins are homogeneously distributed within each compartment and are equally segregated between mother and daughter cells. We describe two exceptions where old and new components either remain separated in distinct domains (nuclear pore complex; NPC) or are asymmetrically inherited (spindle pole body; SPB). Our comprehensive analysis of inheritance of intracellular compartments defines general rules of equal partitioning of constituent proteins and some exceptions where daughters found a different solution to obtaining their essential biological share.

Results

Generation of a Collection of Yeast Strains for Intracellular Compartment Tracing.

We have recently developed a system to distinguish old and new proteins, named RITE. It consists of an inducible Cre-recombinase (which can be activated at will with β-estradiol) and a DNA tagging cassette that can be introduced in the genetic locus of the gene of interest (Fig. 1). Here we used a RITE DNA cassette with a GFP tag flanked by two LoxP recombination sites and followed by a red fluorescent protein (RFP) tag. This allows us to distinguish proteins produced before Cre activation (GFP-labeled) from newly synthesized proteins (RFP-labeled) following the "genetic switch" in single cells.

We generated a collection of RITE haploid *S. cerevisiae* by tagging proteins representative of each intracellular compartment (Fig. S1A). The target proteins were selected on the basis of the following characteristics: (i) essential cellular function, (ii) conservation among eukaryotes, (iii) slow turnover rate, and (iv) lack of effects on cell viability resulting from C-terminal GFP or RFP fusion. With the exception of the nucleolar marker, we chose proteins integrated in the membrane of organelles to exclude exchange by dynamic diffusion. The Yeast GFP Fusion Localization Database (http://yeastgfp.yeastgenome.org) was a source for selection of candidate genes allowing the GFP modification (17, 18). The RITE cassette was incorporated at the endogenous locus of target genes, yielding physiological expression of RITE-tagged proteins without competition from untagged

Fig. 1

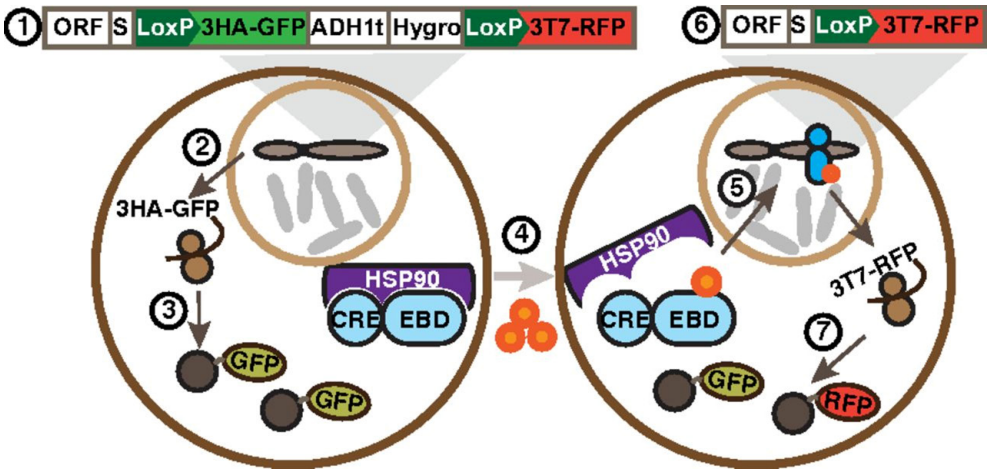

Figure 1: Schematic representation of RITE.
(1) In-frame insertion of RITE DNA with the ORF of the target gene. RITE DNA contains two tags (3HA-GFP and 3T7-RFP) separated by two LoxP recombination sites, an invariant flexible spacer (S), a transcriptional terminator (ADH1t), and a hygromycin resistance gene (Hygro). (2 and 3) As a result, the protein of interest is tagged with LoxP-3HA-GFP. (4–6) RITE yeasts express Cre-recombinase fused to the estrogen-binding domain (Cre-EBD), which is kept inactive binding to Hsp90. β-Estradiol releases Cre-EBD that then enters the nucleus for DNA recombination, resulting in a tag switch to LoxP-3T7-RFP. (7) The genetic switch yields proteins tagged with LoxP-3T7-RFP.

proteins.

To monitor protein inheritance, the genetic switch was induced during the postdiauxic shift (PDS) (Fig. S1 B–D). The PDS is naturally reached when the glucose in the media is consumed, resulting in adjustment of metabolism, low protein synthesis, the ability to remain viable for long periods of time, and very slow proliferation (one doubling over a period of days) (19). Once the genetic switch was completed, fresh medium was added to synchronously induce the first cell division within 3–4 h (Fig. S1D). We measured the levels of mRNA for the GFP-labeled proteins (GFP-mRNA) for each RITE strain (Fig. S2 and Table S1). GFP-mRNAs were unstable after the genetic switch and degraded during the PDS or within 30 min after release into fresh media. Therefore, (old) GFP-mRNAs do not contribute to the synthesis of new proteins during the first cell division in released cells. To monitor protein inheritance, we visualized old (GFP) and new (RFP) proteins by time-lapse microscopy and analyzed their final distribution at anaphase (3 h postrelease). For the study of highly dynamic organelles, such as the Golgi, the genetic switch was performed in log phase (Fig. S1 E–G).

RITE allowed us to perform a pulse–chase type of experiment in intact cells, where old and new proteins can be monitored by fluorescent microscopy. Unlike classical pulse–chase protocols, RITE can be combined with cell division, as done here, and with genetic screens (20).

Old and New Proteins Are Homogeneously Distributed in Most Organelles.

Tracing organelle markers for nucleolus, ER, mitochondria, vacuoles, and Golgi with RITE revealed even distribution between mother and bud. New proteins were uniformly

incorporated along with old proteins, as shown by the overlapping distribution of GFP and RFP (Fig. 2A). Quantification of GFP fluorescence intensity revealed that daughter cells inherited half of the old maternal proteins (Fig. 2B). Likewise, incorporation of new material reached comparable levels in mother and bud pairs, as deduced from the RFP fluorescence signal. The distribution of GFP and RFP was confirmed by immunofluorescence, as shown

Fig. 2

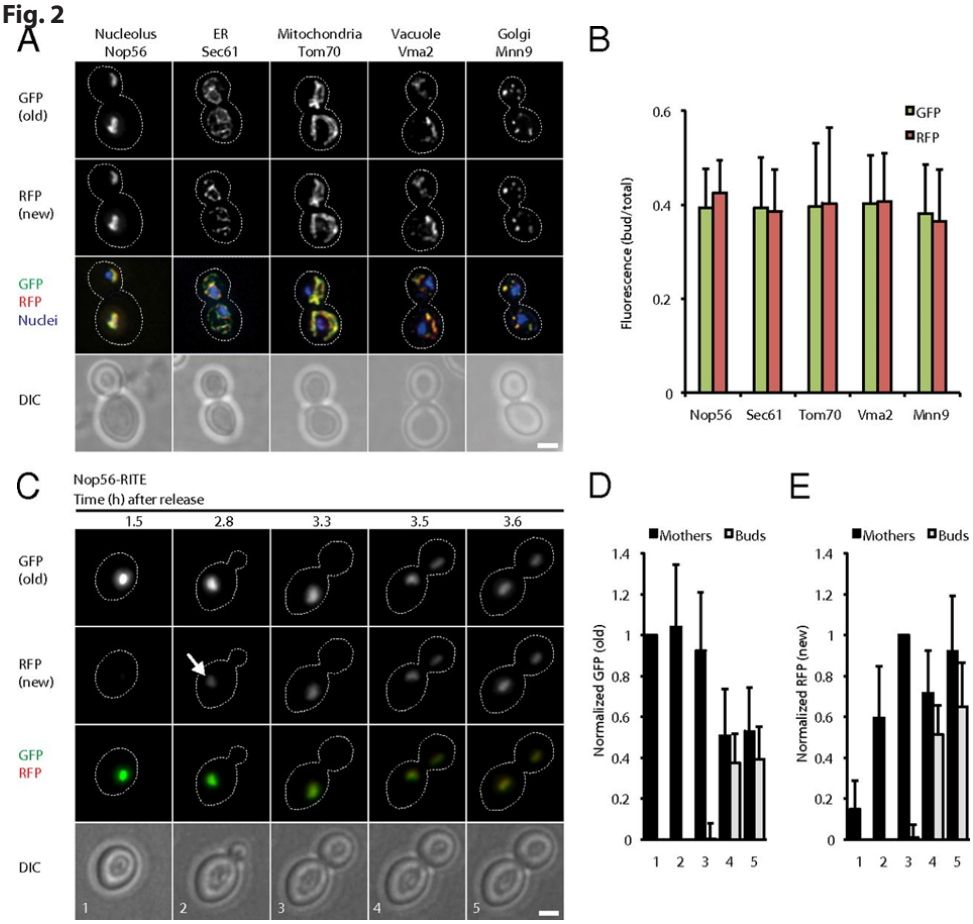

Figure 2: Nucleolus, ER, mitochondria, vacuole, and Golgi segregate symmetrically during cell division.

(A) Representative images of RITE strains 3 h postrelease. For the Golgi, the genetic switch was performed in log phase. (B) Quantification of old (GFP) and new (RFP) proteins at 3 h postrelease, measured as indicated in Materials and Methods. Values are average ± SD, determined from 25, 52, 32, 35, and 30 dividing cells, respectively (n). (C) Selected frames from time-lapse recordings of Nop56-RITE starting at 1 h postrelease. Images were taken at 10-min intervals over 3.5 h. The selected frames correspond to the following cell-cycle stages: (1) start, (2) bud emergence, (3) bud growth, (4) nuclear division, and (5) anaphase. The time (h) elapsed since the release is indicated by the numbers above the frames. The arrow indicates the area where new (RFP) Nop56 appears. (D and E) Quantification of old (GFP) and new (RFP) Nop56 in time-lapse recordings, imaged as indicated in C. For each dividing cell, frames were selected for the different cell-cycle stages (1–5), and GFP (D) and RFP (E) were measured in mother and daughter cells. GFP measurements were normalized to GFP in the mother cell in the first frame (1), and RFP measurements were normalized to RFP in the mother cell at bud-growth stage (3). Values are average ± SD (n = 26 cells). For all of the images, dashed lines represent the cell outlines based on DIC images. (Scale bars, 2 µm.) DIC, differential interference contrast.

for Vma2-RITE (Fig. S3). Time-lapse microscopy revealed similar dynamics of old and new proteins during cell division for these organelles (Fig. 2C and Fig. S4). With the exception of the Golgi, the total pool of old (GFP) proteins remained constant during cell division. When organelles segregated into the bud, old (GFP) proteins were redistributed between mother and daughter cells and remained thereafter (Fig. 2 C and D and Fig. S4 A–C). New (RFP) proteins were first detected in the mother cell, before organelle transfer, and continued increasing in mother and daughter cells during mitosis. The ER marker Sec61 appeared simultaneously in mother and daughter cells after organelle transfer (Fig. S4A). In the Golgi, old (GFP) Mnn9 disappeared following the genetic switch, probably due to the dynamic nature of the Golgi (20, 21). Time-lapse experiments showed exchange by new (RFP) Mnn9 at early phases of division (Fig. S4D).

In summary, nucleoli, ER, mitochondria, vacuole, and Golgi exhibit ordered partitioning and template-based growth, resulting in equal sharing of old and new organelle content between generations.

Peroxisomes Are Duplicated in a Template-Based Manner Before Segregation.

Peroxisomes are duplicated and subsequently segregated during each cell division. The duplication of peroxisomes has been a subject of debate, and two conflicting models have been proposed: *de novo* formation (7–10) and template growth from existing peroxisomes (21).

Fig. 3

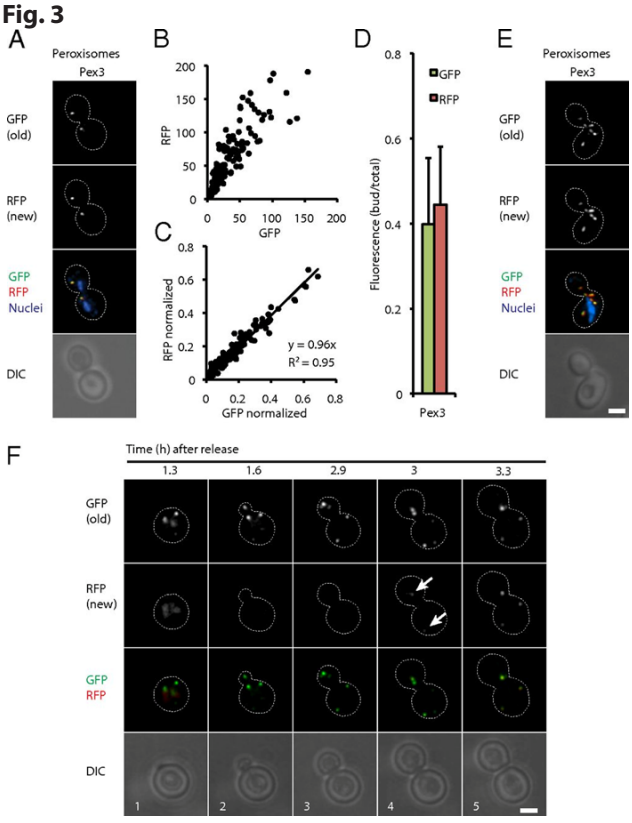

Figure 3: Peroxisomes are duplicated in a template-based manner and are equally segregated between mother and daughter cells. (A) Representative images of Pex3-RITE at 3 h postrelease. (B and C) Quantification of old (GFP) and new (RFP) Pex3 per individual peroxisome, showing total fluorescence intensities (B) and normalized values (C). Each dot represents an individual peroxisome (n = 120 peroxisomes, 22 dividing cells). (D) Quantification of old (GFP) and new (RFP) Pex3 at 3 h postrelease. Values are average ± SD (n = 30 dividing cells). (E) Representative images of Pex3-RITE, 3 h after inducing the genetic switch during cell division. (F) Selected frames from time-lapse recordings of Pex3-RITE, starting 1 h postrelease. Images were taken at 10-min intervals over 3.5 h. The selected frames correspond to the following cell-cycle stages: (1) start, (2) bud emergence, (3) bud growth, (4) nuclear division, and (5) anaphase. The time (h) elapsed since the release is indicated by the numbers above the frames. The arrows indicate the areas where new (RFP) Pex3 appears. For all of the images, dashed lines represent the cell boundaries based on DIC images. (Scale bars, 2 μm.)

We tagged an early integral peroxisomal membrane protein, Pex3 (22), with the RITE cassette and monitored the incorporation of newly synthesized Pex3 in peroxisomes. In the majority of cases (~99% of peroxisomes analyzed), newly synthesized (RFP) Pex3 was only present in peroxisomes containing preexisting (GFP) Pex3 (Fig. 3A). Quantification of GFP and RFP fluorescence intensities revealed that peroxisomes contained different quantities of Pex3. However, the relative amounts of old versus new Pex3 per peroxisome after one cell division was constant, as indicated by the linear correlation between GFP and RFP (Fig. 3 B and C). Old and new Pex3 were equally shared after cell division (Fig. 3D). Similar results for peroxisomal growth and segregation were found in experiments where the genetic switch was performed in log phase (Fig. 3E). Finally, the dynamics of Pex3 were visualized after a genetic switch in PDS by time-lapse imaging (Fig. 3F). Transfer of peroxisomes to the bud started early in mitosis and the total pool of old (GFP) Pex3 remained constant. By contrast, new (RFP) Pex3 was detected later and increased toward the end of anaphase. Importantly, new (RFP) Pex3 appeared (and remained) only in peroxisomes that were already labeled with Pex3-GFP. *De novo* synthesis of peroxisomes would have shown peroxisomes with exclusively new (RFP) Pex3, which was not observed. Rather, all peroxisomes contained both old and new Pex3 after cell division, supporting a template-based model of peroxisome duplication. Early transfer of peroxisomes to the daughter cell and template-based growth of peroxisomes resulted in equal distribution of old and new Pex3 in mitosis.

Old and New NPCs Are Equally Segregated Without Mixing.

The nuclear envelope is a specialized case in organelle inheritance. In yeast, unlike mammalian cells, the nuclear envelope does not break down during mitosis but segregates alongside the chromosomes followed by fission (23). It is unclear whether the components of the nuclear envelope are freely distributed between mother and daughter cells. In particular, the segregation of NPCs is controversial, with two opposing models currently dominating the field. On the basis of photobleaching experiments it has been suggested that preexisting NPCs are retained by the mother cell, whereas only new NPCs are incorporated into the bud (24). By contrast, experiments with nucleoporins tagged with a photoconvertible fluorescent protein suggested that maternal NPCs migrate into the daughter cell (25).

We tagged two nucleoporins, Nup57 and Nup188, with RITE. These represent a central channel protein and a structural component of the NPC, respectively (26). The RITE assay showed that both preexisting (from maternal origin) and newly synthesized nucleoporins were present in mother and daughter cells (Fig. 4A). Quantification of old and new nucleoporins revealed an equal distribution among mothers and buds (Fig. 4B). Although maternal nucleoporins were shared with the bud, old and new nucleoporins did not mix, resulting in alternating regions formed by only old NPCs and only new NPCs (Fig. 4C). Strikingly, the old NPCs excluded new (RFP) Nup57 or Nup188 across generations, indicating that, once assembled, NPCs are very stable macromolecular complexes (Fig. 4D). We followed the dynamics of Nup57 inheritance by time-lapse microscopy (Fig. 4 E–H). At nuclear division, ~40% of old (GFP) Nup57 was transferred from the mother to the daughter cell and remained constant thereafter (Fig. 4 E and F). New (RFP) Nup57 appeared in the mother cell before nuclear division (Fig. 4E). As RFP has a lower quantum yield than GFP, new Nup57 may be more poorly detected. Therefore, we generated a strain with Nup57 tagged with T7 (nonfluorescent) that could be switched to HA-GFP (Fig. 4 G

and H). New (GFP) Nup57 appeared in the mother cell early after the switch (2 h), at the initiation of the cell cycle, and reached maximum levels before nuclear division. At nuclear division, ~40% of new (GFP) Nup57 was transferred to the daughter cell. Importantly, synthesis and incorporation of new Nup57 continued beyond nuclear division in both mother and daughter cells.

In conclusion, our data support a model where preexisting NPCs are highly stable and segregate equally between mother and daughter cells (25), whereas new NPCs are assembled *de novo* in both cells throughout cell division.

Fig. 4

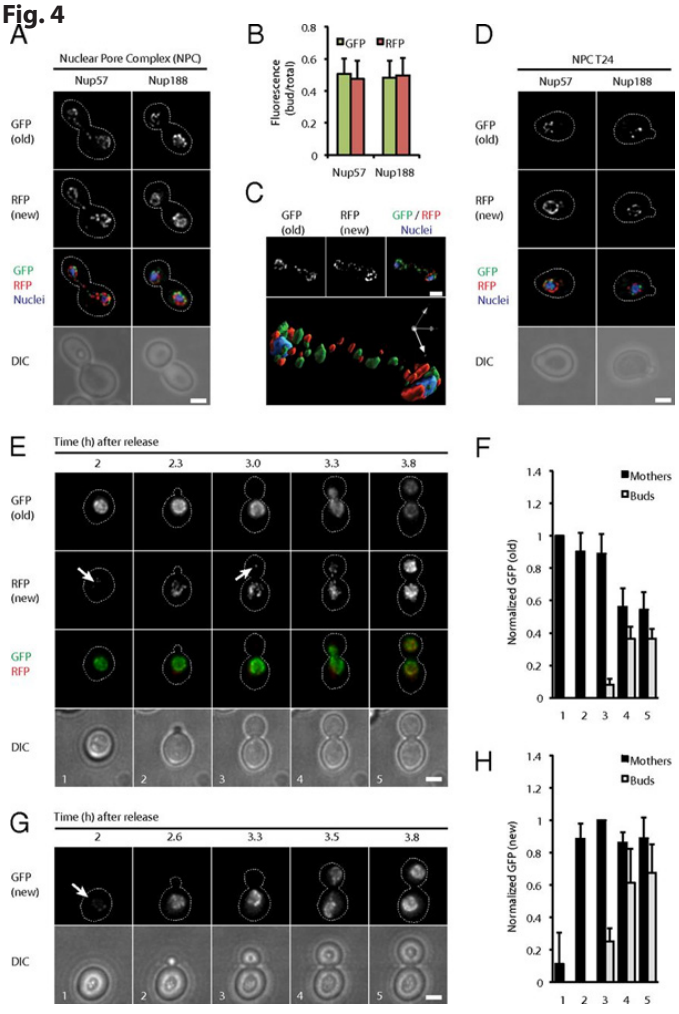

Figure 4 Old and new nucleoporins segregate equally between mother and daughter cells without mixing. (A) Representative images of Nup57-RITE and Nup188-RITE at 3 h postrelease. (B) Quantification of old (GFP) and new (RFP) Nup57 and Nup188 at 3 h postrelease. Values are average ± SD (n = 20 and 26 dividing cells). (C) Representative image of Nup57-RITE at 3 h postrelease. The image was acquired using structured illumination; a z projection (Upper) and the corresponding 3D-rendering model (Lower) are shown. Arrows represent the x-y-z axes. (D) Representative images of Nup47-RITE and Nup188-RITE 24 h (six cell divisions) postrelease. (E) Selected frames from time-lapse recordings of Nup57-RITE starting 1 h postrelease. Images were taken at 10-min intervals over 3.5 h. The selected frames correspond to the following cell-cycle stages: (1) start, (2) bud emergence, (3) bud growth, (4) nuclear division, and (5) anaphase. The time (h) elapsed since the release is indicated by the numbers above the frames. The arrows indicate the area where new (RFP) Nup57 appears. (F) Quantification of old (GFP) Nup57 in time-lapse recordings, imaged as indicated in E. For each dividing cell, frames were selected for different cell-cycle stages (1–5) and GFP was measured in mother and daughter cells. GFP measurements were normalized to GFP in the mother cell in the first frame (1). Values are average ± SD (n = 32 cells). (G) Nup57 was tagged with an alternative RITE cassette consisting of an epitope switch from T7 (nonfluorescent) to HA-GFP. Time-lapse imaging was performed and is represented as indicated in E. Arrows indicate the location of newly formed Nup57 (GFP). (H) Quantification of new (GFP) Nup57 in time-lapse recordings, imaged as indicated in G. For each dividing cell, frames were selected for different cell-cycle stages (1–5) and GFP was measured in mother and daughter cells. GFP measurements were normalized to GFP in the mother cell at bud-growth stages (3). Values are average ± SD (n = 30 cells). For all of the images, dashed lines represent the cell boundaries based on DIC images. (Scale bars, 2 μm.)

RITE Reveals a Unique Pattern for SPB Duplication and Inheritance.
One known exception to equal sharing between subsequent generations is the SPB—the centrosome in yeast (27–29). The SPB is a large protein complex embedded in the nuclear envelope (30). Each cell cycle, the SPB duplicates and each resulting SPB migrates to opposite sites of the nucleus to form the mitotic spindle. SPB duplication has been described as a conservative process that generates one old and one new SPB, followed by migration of the old SPB to the daughter cell (27). However, a later study suggested that the SPB is a dynamic complex that grows and exchanges subunits during cell division (28). Thus, the duplication process may be more complex than previously reported.
The RITE technology allowed monitoring SPB duplication and inheritance by tagging two different core SPB proteins, Spc42 and Spc110. The old (GFP) SPB components were asymmetrically distributed toward the bud, with only a small proportion remaining in mother cells (Fig. 5A). Remarkably, new proteins were incorporated into both SPBs. Quantification of the fluorescence intensity of old and new SPB subunits showed that most old subunits (~90%) were inherited by the daughter cell, whereas new subunits were incorporated to approximately the same extent into both SPBs (Fig. 5B). An alternative RITE construct with an epitope switch from GFP to mCherry (30) showed identical results (Fig. S5).
We followed the dynamics of SPB duplication by time-lapse imaging Spc42-RITE (Fig. 5C). The duplication started when a small proportion of old (GFP) Spc42 was separated from the original SPB and formed a small SPB. During the cell cycle, both SPBs continuously grew, incorporating new (RFP) Spc42. Notably, the total amount of old (GFP) Spc42 remained constant during the SPB growth, which is different from the exchange process described earlier (28).
Our data suggest that the SPB is duplicated following a unique pattern that is neither conservative nor semiconservative and that is followed by the transfer of the older SPB to the younger cell (Fig. 5D).

Discussion

The process of sharing copies of DNA in a correct manner in cell division has been recognized as essential for cell viability for a long time. Correct sharing of compartments and multiprotein complexes is also vital for successful progeny but is poorly described in many instances. How intracellular compartments grow and segregate during cell division has been visualized with inducible expression strategies and fluorescent reporters and by monitoring steady-state levels. These experiments have improved our understanding of protein inheritance but have also produced controversial results. We visualized compartment and multiprotein complex inheritance in a more global manner using a "genetic color switch" in yeast. This genetic switch is an *in vivo* pulse–chase assay with the advantage of a readout on protein destiny by fluorescent microscopy, which allows spatiotemporal analysis of the fate of old and new proteins. The fact that a genome-wide GFP-knockin library in yeast is available in the public domain allows accurate prediction of genes that can safely be modified by the RITE cassette (17, 18). Knocking in this genetic color switch within a collection of genes that represent essential and stable components of each intracellular compartment allowed a comprehensive analysis of the spatiotemporal fate of intracellular compartments during cell division.

Fig. 5

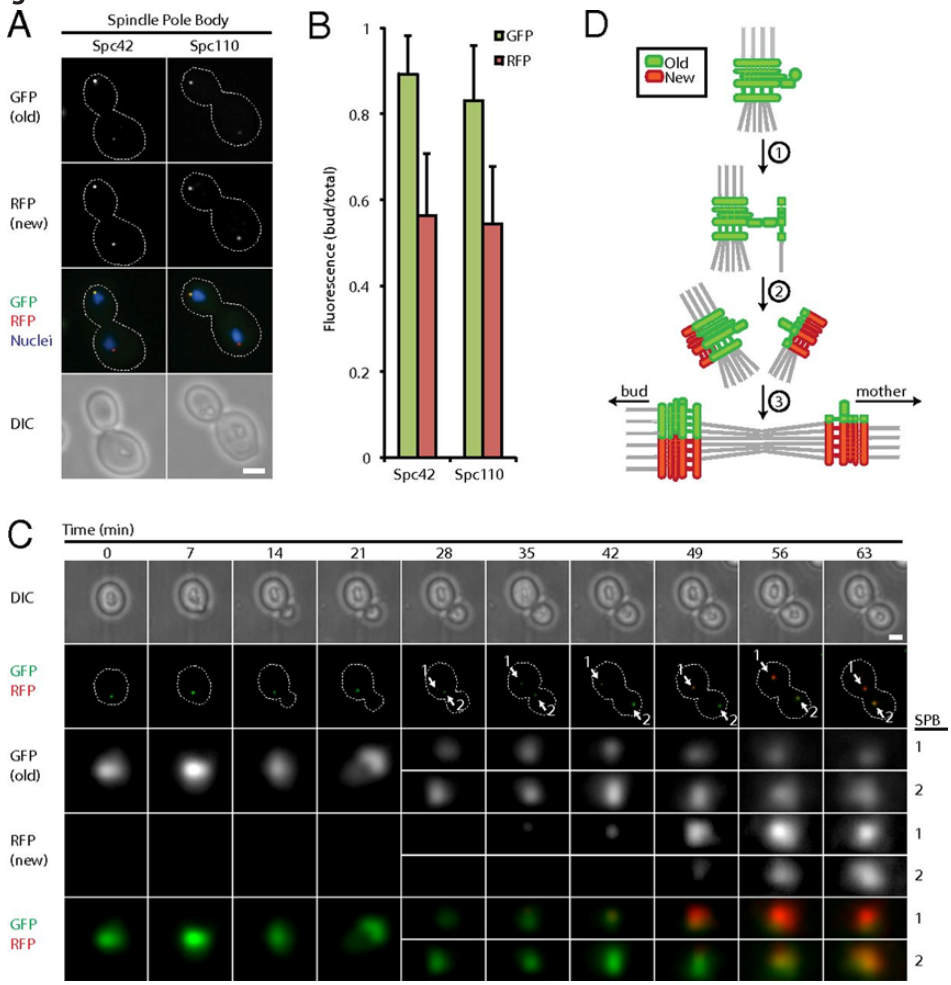

Figure 5: The SPB duplicates by a nonconservative mechanism followed by asymmetrical segregation between mother and daughter cells.

(A) Representative images of Spc42-RITE and Spc110-RITE at 3 h postrelease. (B) Quantification of old (GFP) and new (RFP) Spc42 and Spc110 at 3 h postrelease. Values are average ± SD (n = 30 dividing cells). (C) Selected frames from time-lapse recordings of Spc42-RITE. The time (h) elapsed since the release is indicated by the numbers above the frames. The new (1) and old (2) SPBs are indicated by arrows, and zoomed-in (8×) in the lower panels. For all of the images, dashed lines represent the cell boundaries based on DIC images. (Scale bars, 2 μm.) (D) Model of SPB duplication and inheritance

Using this technology, we showed that most organelles grow by homogeneous incorporation of new proteins into preexisting templates. These include several membrane-associated compartments (ER, mitochondria, vacuole, the Golgi apparatus) and the nucleolus. This growth pattern was also observed for peroxisomes. We noted that newly synthesized Pex3 was incorporated into preexisting peroxisomes, whereas peroxisomes exclusively containing new Pex3 were not observed. New Pex3 stayed connected to preexisting peroxisomes, resulting in a similar proportion of old and new Pex3. Collectively, our observations support template-based growth as the dominant

pathway for peroxisomal biogenesis, as observed for most other compartments, resolving a long-standing controversy in the field.

Although mother and daughter cells share and mix most of their organelles, some exceptions were observed relating to two stable macromolecular complexes within the nuclear envelope: the NPC and the SPB. Both old and new NPCs were present in mother and daughter cells, but the complexes remained spatially separated. Although shared between mother and daughter, NPCs are very stable complexes that do not renovate their subunits even after many divisions. New NPCs are assembled *de novo* using new nucleoporins. The SPB is a large and also stable multiprotein complex, yet, unlike the NPC, the already-assembled SPB allows incorporation of new proteins, an observation differing from previous descriptions (27, 29). Pereira and coworkers (27) exploited the slow maturation of RFP to follow old Spc42, reasoning that new Spc42-RFP acquires fluorescence only during the next cell cycle. To monitor new Spc42, they used inducible expression driven by the GAL promoter. We could—using RITE—follow SPB duplication without changing the endogenous regulation of SPB synthesis, which may explain the discrepancy in observations.

Based on our data, we propose a model for SPB biogenesis (Fig. 5D). First, a small proportion of maternal SPB components splits to initiate the duplication process. Newly synthesized proteins are added to this template to build the new SPB. Simultaneously, new proteins are also incorporated into the original SPB that consequently increases in size. Finally, as the cell cycle progresses, the original SPB—containing most of the preexisting components—migrates into the daughter cell. Consequently, the size of the SPB in mother cells may eventually become smaller than in daughter cells (which contains most of the old—and an equal number of new—SPB components). There are at least two options that could explain these results: One is to compensate for the difference in SPB size with synthesis and/or degradation in mother and daughter cells after cytokinesis. Alternatively, the shrinkage of the SPB in the mother yeast may be irreversible, which may ultimately restrict the lifetime of old yeast.

We have used a unique technology to study the fate and inheritance of all organelles and some large protein complexes. Mother cells usually share their content with daughter cells during cell division, with some exceptions where maternal components are kept separated from the new proteins or where old quality-controlled and functional components may be preferentially inherited by daughter cells.

Materials and Methods

Plasmids, yeast strains, growth conditions, RT-quantitative PCR, sample preparation for microscopy analysis, and immunofluorescence are described in SI Materials and Methods. The genetic switch was induced by adding β-estradiol (E-8875; Sigma-Aldrich) to a final concentration of 1 μM.

Fixed samples were analyzed with a Leica DMI 60000B wide-field fluorescence microscope equipped with a structural light unit (Angstrom Optigrid, Quorum Technologies) and using a Leica HCX PlanApo 63×/1.4–0.6 oil objective. Images were taken as z stacks (20 sections at 0.2-μm intervals). When indicated, the unit for structural illumination was used (40 sections at 0.1-μm intervals). Images were deconvolved using Volocity (Improvision/PerkinElmer) software (99% confidence limit per 25 iterations) with calculated point-spread functions for each wavelength. Three-dimensional structures were obtained using

high-resolution volume rendering (Volocity). For quantification, we used Volocity software to measure the integrated GFP and RFP intensities and the background fluorescence (minimal fluorescence intensity) for each cell and marker. The relative (bud/total) GFP intensity was calculated for each mother–bud pair as follows: GFPbud/total = (GFPb − GFP0)/[(GFPb − GFP0) + (GFPm − GFP0)], where b is the bud, 0 is the background, and m is the mother. This formula was also used to calculate the RFPbud/total. For quantification of peroxisomes, the GFP intensities of each individual peroxisome were normalized as follows: GFP = (GFPp − GFP0)/SUM_GFP, where p is the peroxisome, 0 is the background, and SUM_GFP is the sum of the GFP intensities (background-subtracted) of all of the peroxisomes within the mother–bud pair. This formula was also applied to calculate normalized RFP intensities.

Time-lapse fluorescent microscopy was performed with a DeltaVision wide-field microscope (Olympus IX70; Applied Precision). Images were acquired at 32 °C as z stacks (10 sections at 0.4-μm intervals) and analyzed using softWoRx software (Applied Precision).

References

1. Fagarasanu A, Mast FD, Knoblach B, Rachubinski RA. Molecular mechanisms of organelle inheritance: Lessons from peroxisomes in yeast. Nat Rev Mol Cell Biol. 2010;11(9):644–654.
2. Bretscher A. Polarized growth and organelle segregation in yeast: The tracks, motors, and receptors. J Cell Biol. 2003;160(6):811–816.
3. Shaw SL, Yeh E, Maddox P, Salmon ED, Bloom K. Astral microtubule dynamics in yeast: A microtubule-based searching mechanism for spindle orientation and nuclear migration into the bud. J Cell Biol. 1997;139(4):985–994.
4. Finger FP, Hughes TE, Novick P. Sec3p is a spatial landmark for polarized secretion in budding yeast. Cell. 1998;92(4):559–571.
5. Boldogh IR, Ramcharan SL, Yang HC, Pon LA. A type V myosin (Myo2p) and a Rab-like G-protein (Ypt11p) are required for retention of newly inherited mitochondria in yeast cells during cell division. Mol Biol Cell. 2004;15(9):3994–4002.
6. Fagarasanu M, Fagarasanu A, Tam YY, Aitchison JD, Rachubinski RA. Inp1p is a peroxisomal membrane protein required for peroxisome inheritance in *Saccharomyces cerevisiae*. J Cell Biol. 2005;169(5):765–775.
7. Hoepfner D, Schildknegt D, Braakman I, Philippsen P, Tabak HF. Contribution of the endoplasmic reticulum to peroxisome formation. Cell. 2005;122(1):85–95.
8. Tam YY, Fagarasanu A, Fagarasanu M, Rachubinski RA. Pex3p initiates the formation of a preperoxisomal compartment from a subdomain of the endoplasmic reticulum in *Saccharomyces cerevisiae*. J Biol Chem. 2005;280(41):34933–34939.
9. Kragt A, Voorn-Brouwer T, van den Berg M, Distel B. Endoplasmic reticulum-directed Pex3p routes to peroxisomes and restores peroxisome formation in a *Saccharomyces cerevisiae* pex3Delta strain. J Biol Chem. 2005;280(40):34350–34357.
10. van der Zand A, Gent J, Braakman I, Tabak HF. Biochemically distinct vesicles from the endoplasmic reticulum fuse to form peroxisomes. Cell. 2012;149(2):397–409.
11. Bevis BJ, Hammond AT, Reinke CA, Glick BS. *De novo* formation of transitional ER sites and Golgi structures in Pichia pastoris. Nat Cell Biol. 2002;4(10):750–756.
12. Liu B, *et al*. The polarisome is required for segregation and retrograde transport of protein aggregates. Cell. 2010;140(2):257–267.
13. Eldakak A, *et al*. Asymmetrically inherited multidrug resistance transporters are recessive determinants in cellular replicative ageing. Nat Cell Biol. 2010;12(8):799–805.
14. van den Bogaart G, Meinema AC, Krasnikov V, Veenhoff LM, Poolman B. Nuclear transport factor directs localization of protein synthesis during mitosis. Nat Cell Biol. 2009;11(3):350–356.
15. De Vos D, *et al*. Progressive methylation of ageing histones by Dot1 functions as a timer. EMBO Rep. 2011;12(9):956–962.
16. Verzijlbergen KF, *et al*. Recombination-induced tag exchange to track old and new proteins. Proc Natl Acad Sci USA. 2010;107(1):64–68.
17. Ghaemmaghami S, *et al*. Global analysis of protein expression in yeast. Nature. 2003;425(6959):737–741.
18. Huh WK, *et al*. Global analysis of protein localization in budding yeast. Nature. 2003;425(6959):686–691.
19. Gray JV, *et al*. "Sleeping beauty": Quiescence in *Saccharomyces cerevisiae*. Microbiol Mol Biol Rev. 2004;68(2):187–206.

20. Verzijlbergen KF, *et al*. A barcode screen for epigenetic regulators reveals a role for the NuB4/HAT-B histone acetyltransferase complex in histone turnover. PLoS Genet. 2011;7(10):e1002284.
21. Motley AM, Hettema EH. Yeast peroxisomes multiply by growth and division. J Cell Biol. 2007;178(3):399–410.
22. Fujiki Y, Matsuzono Y, Matsuzaki T, Fransen M. Import of peroxisomal membrane proteins: The interplay of Pex3p- and Pex19p-mediated interactions. Biochim Biophys Acta. 2006;1763(12):1639–1646.
23. Mekhail K, Moazed D. The nuclear envelope in genome organization, expression and stability. Nat Rev Mol Cell Biol. 2010;11(5):317–328.
24. Shcheprova Z, Baldi S, Frei SB, Gonnet G, Barral Y. A mechanism for asymmetric segregation of age during yeast budding. Nature. 2008;454(7205):728–734.
25. Khmelinskii A, Keller PJ, Lorenz H, Schiebel E, Knop M. Segregation of yeast nuclear pores. Nature. 2010;466(7305):E1.
26. Hoelz A, Debler EW, Blobel G. The structure of the nuclear pore complex. Annu Rev Biochem. 2011;80:613–643.
27. Pereira G, Tanaka TU, Nasmyth K, Schiebel E. Modes of spindle pole body inheritance and segregation of the Bfa1p-Bub2p checkpoint protein complex. EMBO J. 2001;20(22):6359–6370.
28. Yoder TJ, Pearson CG, Bloom K, Davis TN. The *Saccharomyces cerevisiae* spindle pole body is a dynamic structure. Mol Biol Cell. 2003;14(8):3494–3505.
29. Hotz M, *et al*. Spindle pole bodies exploit the mitotic exit network in metaphase to drive their age-dependent segregation. Cell. 2012;148(5):958–972.
30. Barral Y, Liakopoulos D. Role of spindle asymmetry in cellular dynamics. Int Rev Cell Mol Biol. 2009;278:149–213.

Supplemental Information:

SI Materials and Methods

Plasmids.
A plasmid containing a GFP→mRFP (red fluorescent protein) recombination-induced tag exchange (RITE) cassette was constructed by restriction enzyme-based cloning of PCR fragments to generate the following construct: NotI-spacer-LoxP-KpnI-3xHA-yEGFP-SpeI-ADH1t-BamHI-HygroMX-XbaILoxP-SalI-3xT7-mRFP-BsrGI, as previously described (1). A plasmid containing a T7→GFP RITE cassette was constructed by swapping GFP from pKT127 (2) into pTW081 (3) using HindIII/ BsrgI restriction and ligation to yield the following construct: NotI-spacer-LoxP-KpnI-T7-ADH1t-HygroMX-LoxP-HA-yEGFPBsrGI. A plasmid to generate mCherry→GFP RITE strains has been previously described (4). For constitutive expression of hormone-regulated Cre, Cre-EBD78 (5), the module NATMX_GPD_Cre-EBD78_CYCt was amplified by a three-step overlap PCR from the plasmids pFvL099 and pTW040 (6) and targeted to the lyp1Δ locus by homologous recombination.

Yeast Strains and Growth Conditions.
The GFP→mRFP and T7→GFP RITE strains are derivatives of Y7092 (7) with the following genotypes: MATα his3Δ1 leu2Δ0 ura3Δ0 met15Δ0 can1Δ::STE2pr-Sp_his5 lyp1Δ::NATMX_TDH3pr_Cre-EBD78_CYC1tx::X-RITE, where x is the target gene. The SPC42-mCherry→GFP strain was made by successive transformations of pFA6a-GFP-S65T-KanMX6 (8) and pYB1511(4) in a BY4733his3::HIS3_GPD_ CRE_EBD78 strain. The genotype of the SPC42-mCherry→GFP strain is his3Δ200 leu2Δ0met15Δ0 trp1Δ63 ura3Δ0 his3::HIS3_GPD_CRE_EBD78spc42::
SPC42-LoxP-mCherry-NatNT2-LoxP-GFP-S65T-KanMX6 (2). Yeast cells were grown at 30 °C in rich medium [yeast extract peptone dextrose (YEPD)]. Hygromycin B (200 μg/mL; Invitrogen) was included when growing GFP→mRFP and T7→GFP RITE strains and removed before induction of the genetic switch.

RNA Isolation and RT-Quantitative PCR.
Total yeast RNA was purified from 3×10^7 cells using an RNeasy Kit (Qiagen) according to the manufacturer's protocol. RNA samples were treated with RNase-free DNase (Qiagen), and cDNA was made with Super-Script II reverse transcriptase (Invitrogen). GFP- and ADH1-cDNA was quantified by real-time PCR using Power SYBR Green PCRMaster Mix (Applied Biosystems) and a 7500 Fast Real-Time PCR System. The primers used for quantitative (q)PCR were:
yEGFP_ORF_fwd, 5′-TTTCTGTCTCCGGTGAAGGT-3′;
yEGFP_ORF_rev, 5′-GGCATGGCA GACTTGAAAAA-3′;
ADH1_ORF_II_fwd, 5′-TAGGTTCTTTGGCTGTTCAATACG-3′;
and ADH1_ORF_II_rev, 5′-CGGAAACGGAAACGTTGATGACACCG-3′.

Sample Preparation for Microscopy Analysis.
For analysis of fixed samples, cells were fixed with 4% (vol/vol) formaldehyde, stained with 1 μg/mL Hoechst 33342 (Invitrogen), and mounted with Vectashield solution (Vector Laboratories) onto Con A-coated coverslips. For live-cell imaging, cells were diluted in synthetic liquid media and plated in a Ludin chamber type I (for round coverslips with 18-mm diameter) with a Con A-coated coverslip.

Immunofluorescence.
Cells were fixed for 30 min at 30 °C in 4% (vol/vol) formaldehyde, washed with SP buffer (0.1 M KPO_4, pH 7.5, 1.2 M sorbitol), and resuspended in SP buffer. To remove the cell wall, cells were incubated for 15 min at 30 °C with gentle shaking in SP buffer containing 0.1% (vol/vol) β-mercaptoethanol and lyticase (10 U per 10^7 cells) (Sigma). Spheroplasts were then washed two times in SP buffer and permeabilized in blocking solution [0.1% (vol/vol) Triton-X, 3% (vol/vol) BSA in PBS]. Spheroplasts were immunostained in suspension, using rabbit polyclonal antibodies specific for GFP (anti-GFP immunostaining) or RFP (anti-RFP immunostaining) (9), followed by incubation with Alexa 647-conjugated anti-rabbit antibody (Molecular Probes).

References:

1. De Vos D, *et al*. (2011) Progressive methylation of ageing histones by Dot1 functions as a timer. EMBO Rep 12(9):956–962.
2. Sheff MA, Thorn KS (2004) Optimized cassettes for fluorescent protein tagging in *Saccharomyces cerevisiae*. Yeast 21(8):661–670.
3. Verzijlbergen KF, *et al*. (2010) Recombination-induced tag exchange to track old and new proteins. Proc Natl Acad Sci USA 107(1):64–68.
4. Hotz M, *et al*. (2012) Spindle pole bodies exploit the mitotic exit network in metaphase to drive their age-dependent segregation. Cell 148(5):958–972.
5. Lindstrom DL, Gottschling DE (2009) The mother enrichment program: A genetic system for facile replicative life span analysis in *Saccharomyces cerevisiae*. Genetics 183(2):413–422.
6. Stulemeijer IJ, *et al*. (2011) Dot1 binding induces chromatin rearrangements by histone methylation-dependent and -independent mechanisms. Epigenetics Chromatin 4(1):2.
7. Tong AH, Boone C (2006) Synthetic genetic array analysis in *Saccharomyces cerevisiae*. Methods Mol Biol 313:171–192.
8. Wach A, Brachat A, Alberti-Segui C, Rebischung C, Philippsen P (1997) Heterologous HIS3 marker and GFP reporter modules for PCR-targeting in *Saccharomyces cerevisiae*. Yeast 13(11):1065–1075.
9. Rocha N, *et al*. (2009) Cholesterol sensor ORP1L contacts the ER protein VAP to control Rab7-RILP-p150 Glued and late endosome positioning. J Cell Biol 185(7):1209–1225.

Fig. S1

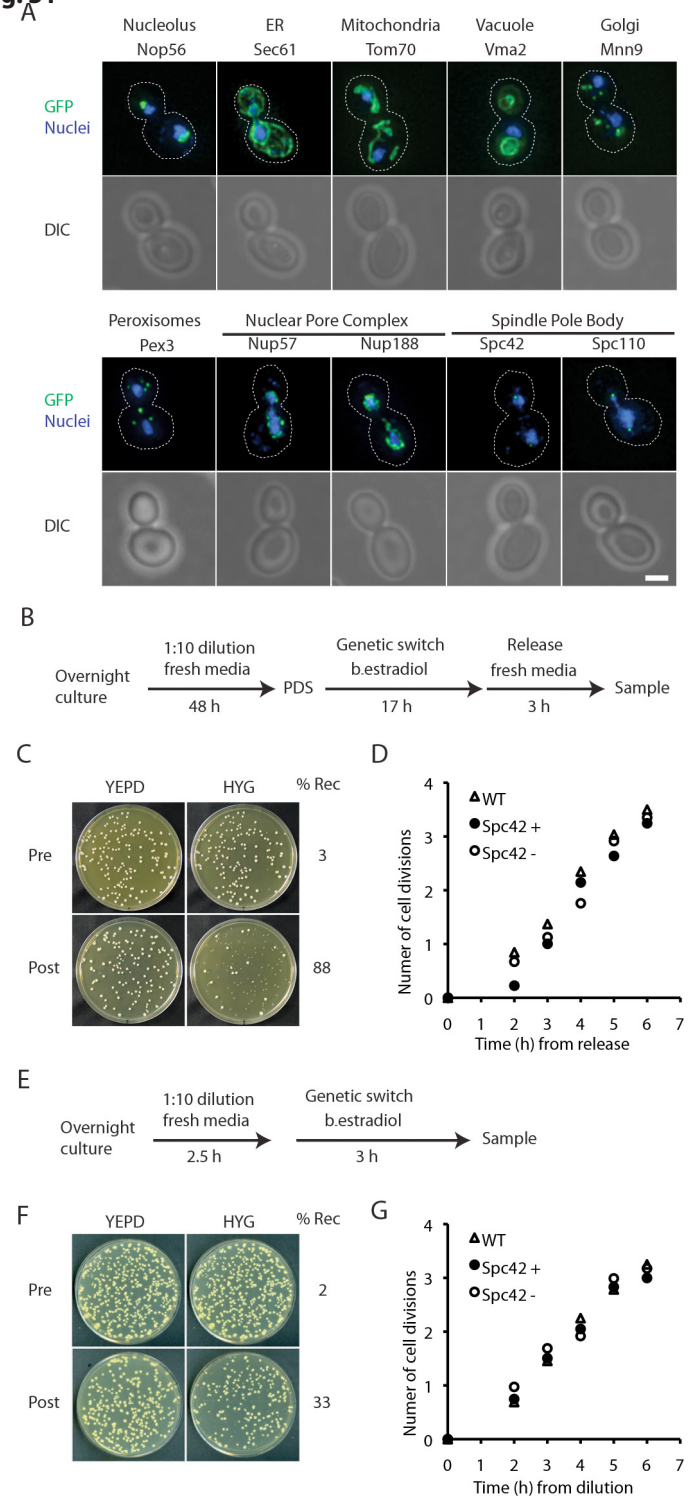

Fig. S1. RITE strains and assays.
(A) Intracellular localization of RITE-tagged proteins in *Saccharomyces cerevisiae*. Dashed lines represent the cell boundaries based on DIC images. ER, endoplasmic reticulum. (Scale bar, 2 μm.) DIC, differential interference contrast. (B–D) Genetic switch during the postdiauxic shift (PDS). (B) Schematic representation of the procedure. (C) Recombination efficiency during the PDS stage. Cells were plated before (Pre) and 17 h after (Post) the genetic switch and replica-plated in control media (YEPD, yeast extract peptone dextrose) or media with hygromycin (HYG). The fraction of hygromycinsensitive colonies indicates the recombination efficiency (Post) and the spontaneous recombination (Pre). (D) Growth rate during the release in fresh media of WT, Spc42-RITE– (without β-estradiol), and Spc42-RITE+ (with β-estradiol). (E–G) The genetic switch in log phase. (E) Schematic representation of the procedure. (F) Recombination efficiency in log phase, before (Pre) and 3 h after (Post) the genetic switch. (G) Growth rate of WT, Spc42-RITE– (without β-estradiol), and Spc42-RITE+ (with β-estradiol). For Spc42-RITE+ cells, β-estradiol was added at 2.5 h, as indicated in E.

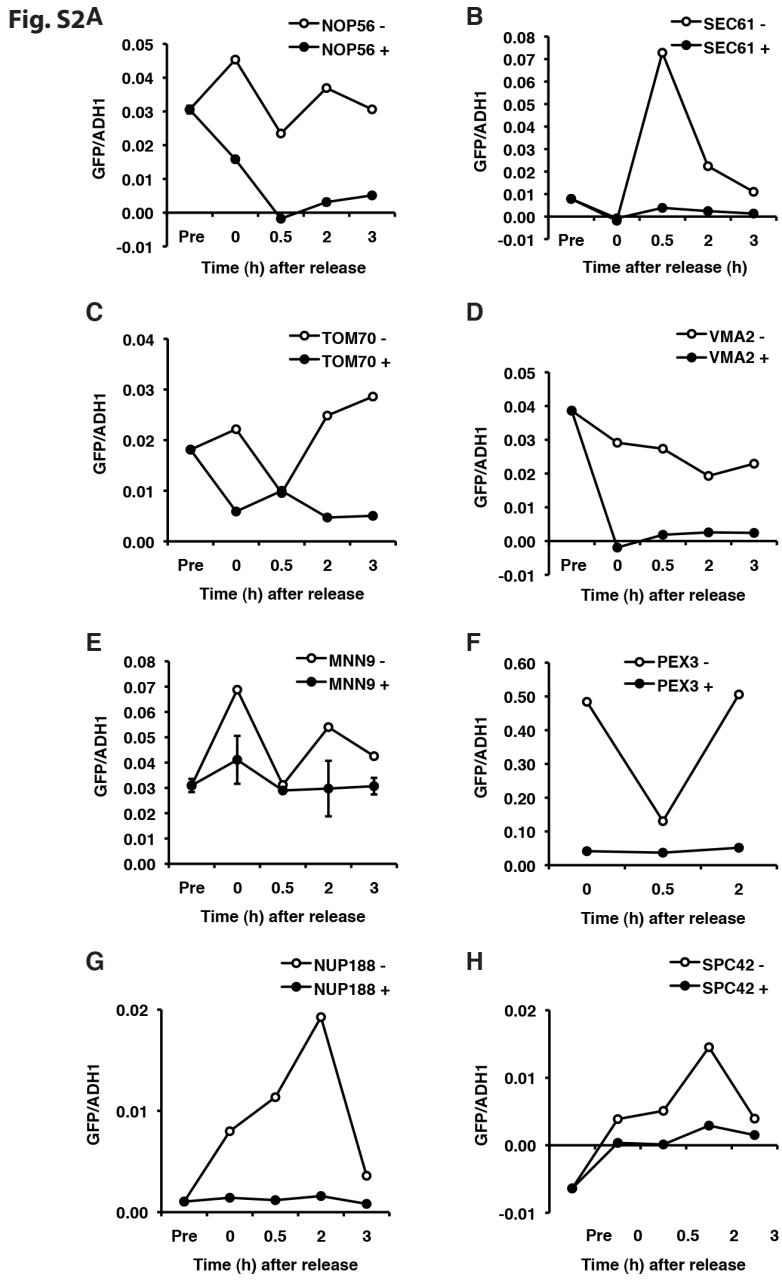

Fig. S2. mRNAs for the GFP-labeled proteins (GFP-mRNA) are degraded after the genetic switch. For each RITE strain used in this study, GFP-mRNA levels were measured by RT-qPCR and normalized to the expression of ADH1 before the switch in PDS (Pre) and at several time points after the release (0, 0.5, 2, and 3 h) by RT-qPCR. GFP RT-qPCR background levels were measured using the Y7092 strain (WT), normalized to the expression of ADH1, and subtracted. Plots show representative curves of biological duplicates for Nop56-RITE (A), Sec61-RITE (B), Tom70-RITE (C), Vma2-RITE (D), Mnn9-RITE (E), Pex3-RITE (F), and Nup188 (G) and Spc42 (H) cells, treated with β-estradiol (+) or without treatment (–). The recombination efficiency was determined in the same experiment for all clones using a plating assay, and the results are shown in Table S1.

Fig. S3

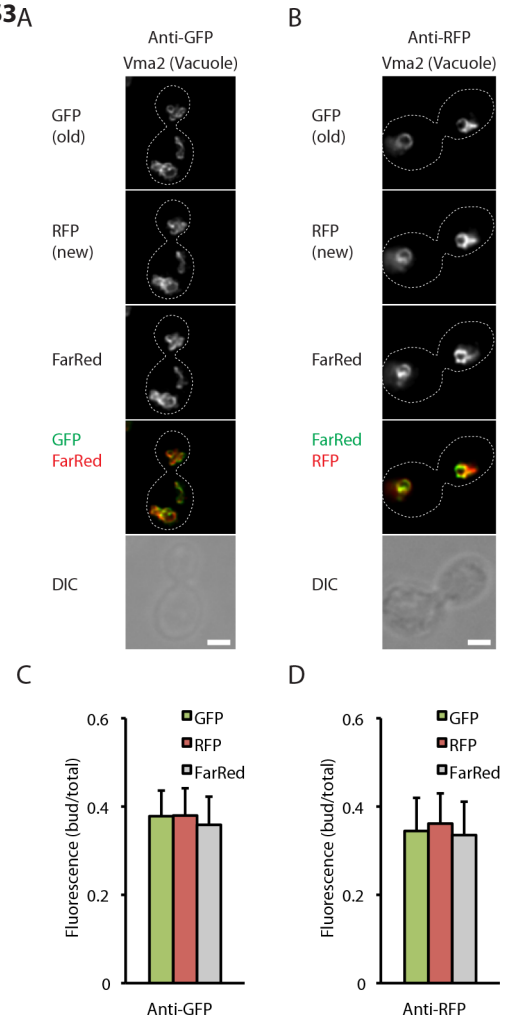

Fig. S3. Segregation of old and new Vma2 proteins shown by immunofluorescence.
Representative images of Vma2-RITE strains 3 h postrelease, immunostained with antibodies specific for GFP (A) and RFP (B) and detected with Alexa 647-conjugated antibody (FarRed). Dashed lines represent the cell boundaries based on DIC images. (Scale bars, 2 µm.) (C) Quantification of GFP, RFP, and FarRed-labeled GFP in cells stained as shown in A. Values are average ± SD (n = 35 dividing cells). (D) Quantification of GFP, RFP, and FarRed-labeled RFP in cells stained as shown in B. Values are average ± SD (n = 35 dividing cells).

Fig. S4

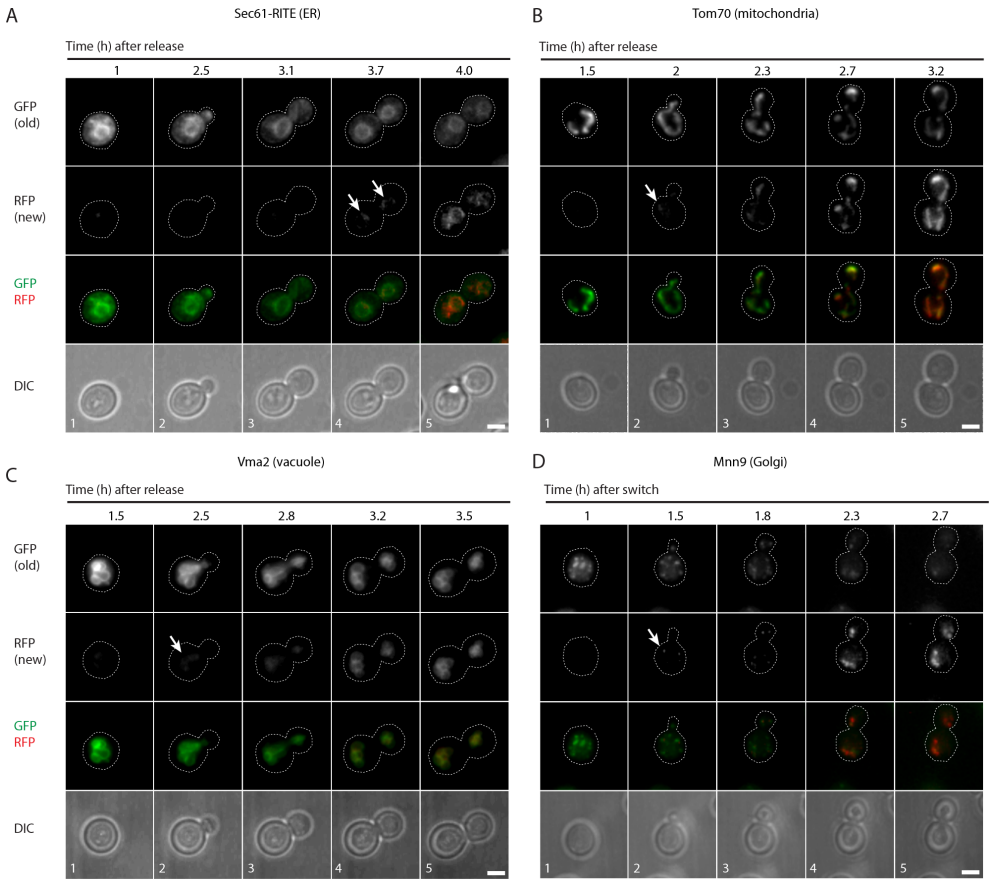

Fig. S4. Time-lapse imaging of the inheritance of ER, mitochondria, vacuole, and Golgi.
Selected time frames from time-lapse recordings of Sec61-RITE (A),Tom70-RITE (B), Vma2-RITE (C), and Mnn9-RITE (D). Live-cell imaging was initiated 1 h postrelease, after a switch performed in stationary phase (A–C) or in log phase (D). Images were taken at 10-min intervals over 3.5 h. The selected frames correspond to the following cell-cycle stages: (1) start, (2) bud emergence, (3) bud growth, (4) nuclear division, and (5) anaphase, and the cell-cycle stages (1–5) are indicated at the bottom. The time (h) elapsed since the release is indicated by the numbers above the frames. The arrows indicate the areas where new (RFP) proteins appear. Dashed lines represent the cell boundaries based on DIC images. (Scale bars, 2 μm.)

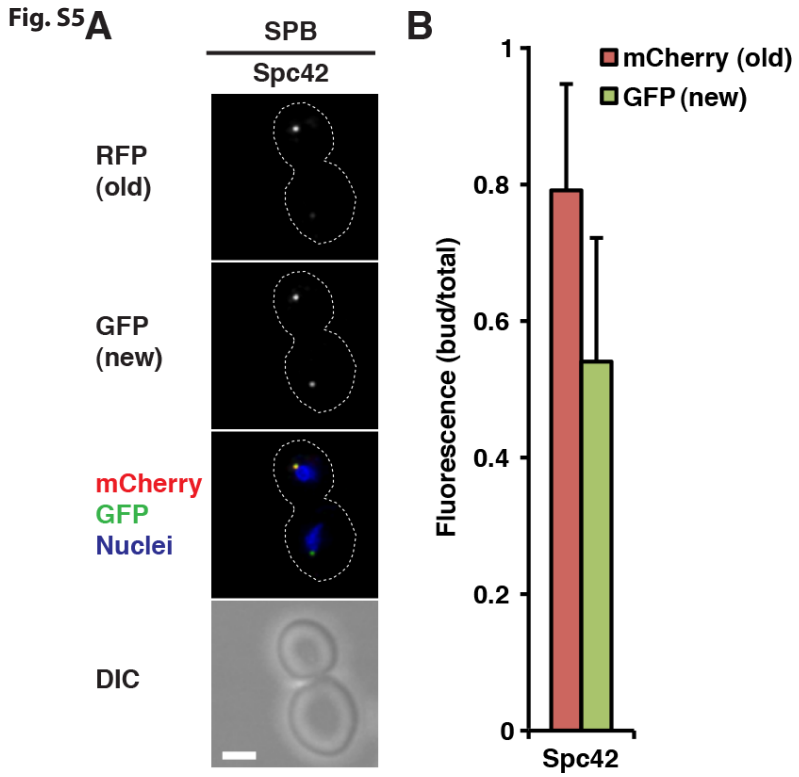

Fig. S5. Duplication and inheritance of Spc42, shown with an alternative RITE cassette, characterized by an epitope switch from mCherry to GFP.
(A) Representative images of Spc42-reRITE 3 h postrelease. Dashed lines represent the cell boundaries based on DIC images. SPB, spindle pole body. (Scale bar, 2 µm.) (B) Quantification of old (mCherry) and new (GFP) Spc42 in mother and daughter cells at 3 h postrelease. Values are average ± SD (n = 24 dividing cells).

Table. S1

	Recombination efficiency (%)	
Strain:	**Pre**	**Post**
Nop56	21	90
Sec61	4	92
Tom70	19	77
Vma2	8	88
Mnn9	14	56
Pex3	12	91
Nup188	18	94
Spc42	17	95

Table S1. Recombination efficiency from all of the RITE clones in the RT-qPCR experiment (Fig. S2)
An aliquot from the cells used for RT-PCR was plated before the switch (Pre) and at time 0, just before the release in fresh media (Post). The spontaneous recombination (Pre) and the recombination efficiency (Post) were calculated as indicated in Fig. S1.